# DNA-modified Artificial Viral Capsids self-assembled from DNA-conjugated $\beta$-Annulus Peptide

Yoko Nakamura, Saki Yamada, Shoko Nishikawa, and Kazunori Matsuura*

Department of Chemistry and Biotechnology, Graduate School of Engineering, Tottori University, Tottori, 680-8552, Japan.

**Abstract**

$\beta$-Annulus peptides from tomato bushy stunt virus conjugated with DNAs ($dA_{20}$ and $dT_{20}$) at the C-terminal were synthesized. The DNA-modified $\beta$-annulus peptides self-assembled into artificial viral capsids with sizes of 45-160 nm. $\zeta$-Potential measurements revealed that the DNAs were coated on the surface of artificial viral capsids. Fluorescence assays indicated that the DNAs on the artificial viral capsids were partially hybridized with the complementary DNAs. Moreover, the DNA-modified artificial viral capsids formed aggregates by adding complementary polynucleotides.

## Introduction

Viral capsids are empty structures of natural viruses, excluding nucleic acids, which can spontaneously self-assemble from viral proteins without infectivity and potential replication probability. The viral capsids as nanoscale materials have been applied to novel drug delivery systems and nanoreactors [1–4]. For example, Douglas and coworkers developed nanoreactors based on alcohol dehydrogenase D encapsulated in bacteriophage P22 capsids [5]. Wang and coworkers reported encapsulation of quantum dots into mutated viral capsids modified with gold nanoparticles on the surface [6]. Conjugation strategies for viral capsids have been developed for display on the exterior surface by biofunctional molecules, such as oligosaccharides and proteins. Finn and co-workers demonstrated the covalent decoration of cowpea mosaic virus (CPMV) with carbohydrate molecules [7]. Kovesdi and co-workers constructed adenovirus particles modified with bispecific antibody to enhance transduction [8].

Oligodeoxyribonucleotides (ODNs) are used as building blocks to construct nanomaterials due to their capability of specific hybridization with the complementary DNA strand [9]. DNA's simple code is able to construct patterned nanostructures in one, two, and three dimensions, which have been used to precisely position proteins and nanoparticles [10]. Recently, surface modification by ODNs on viral capsids has been developed to afford molecular recognition ability to viral capsids. Francis and co-workers

achieved a one-dimensional arrangement of viral capsids modified with ODN strands on DNA origami tiles [11]. Finn and co-workers reported that CPMV capsids modified with ODNs aggregated by mixing with capsid-bearing complementary ODNs [12]. Francis and co-workers constructed cell-targeting vehicles by modification of bacteriophage MS2 capsids with ssDNA aptamers on the surface [13].

On the other hand, rationally designed self-assembled protein/peptide nanostructures have a potential for biomaterial applications, which inspired the development of bottom-up nanotechnology [14, 15]. Woolfson and co-workers demonstrated that two complementary trimeric coiled-coil units can form monolayer spheres of approximately 100 nm in diameter by self-assembly [16]. Ryadnov and co-workers demonstrated that artificial virus-like particles self-assembled from designed peptides can encapsulate nucleic acids [17, 18]. Self-assembled peptide nanospheres have the potential to serve as materials for therapeutic carriers because of their biodegradability. Hashizume and co-workers showed that recombinant protein nanoparticles modified with vascular endothelial cell binding peptide can target cancer cells [19]. However, modification of biofunctional molecules onto the surface of nanospheres self-assembled from rationally designed proteins/peptides is still in its infancy.

We previously demonstrated that a synthetic 24-mer $\beta$-annulus peptide fragment (INHVGGTGGAIMAPVACTRQLVGS), which is a structural motif of the internal skeleton of tomato bushy stunt virus capsid, self-assembled into virus-like nanocapsules (artificial viral capsids) with sizes of 30–50 nm in water [20]. It is also suggested that the C-terminals of the peptides are directed to the surface of the nanocapsules, while the N-terminals are directed towards the interior [21]. These properties made it possible to encapsulate anionic dyes, DNA [21], His-tagged proteins [22], and anionic CdTe quantum dots [23] into the artificial viral capsids. We also constructed artificial viral capsids decorated with gold nanoparticles by C-terminal modification of the $\beta$-annulus peptides [24]. These molecular designs enabled selective modification of artificial virus capsids with functional molecules in the interior and at the surface of capsids.

In the present study, we report the synthesis and self-assembly of artificial viral capsids modified with homopolymeric 20-mer oligodeoxyadenosine ($dA_{20}$) and 20-mer oligothymidine ($dT_{20}$) at the C-terminal of the $\beta$-annulus peptide (Figure 1). The self-assembling behavior of the DNA-modified $\beta$-annulus peptide into the artificial viral capsid was studied by dynamic light scattering (DLS) analyses and transmission electron microscopy (TEM). The hybridization behavior of the DNA-modified artificial viral capsids with the complementary DNAs was examined by fluorescence assays and DLS.

**Results and Discussion**

The synthetic scheme of $dA_{20}$-modified *β*-annulus peptide conjugate (**$dA_{20}$-*β*-annulus**) is shown in Figure 1. The $dA_{20}$ bearing an amino group via a hexamethylene chain at the 5′ end was reacted with the activated ester of a heterofunctional linker, *N*-(4-maleimidobutyryloxy)sulfosuccinimide sodium salt, to introduce a maleimide group to the $dA_{20}$. A *β*-annulus peptide containing Cys at the second position from the C-terminal (INHVGGTGGAIMAPVAVTRQLVCS) was synthesized using a standard Fmoc-protected solid-phase method. Subsequently, **$dA_{20}$-*β*-annulus** was prepared by reaction of the Cys of the peptide with the $dA_{20}$-maleimide, and purified by reversed-phase HPLC. The HPLC retention times of $dA_{20}$-$NH_2$, $dA_{20}$-maleimide, and *β*-annulus Cys peptide are 22 min, 24.5 min and 42 min, respectively (Figure 2A). The $dA_{20}$-modified *β*-annulus peptide showed one main peak at 35.5 min (Figure 2A (d)), which was confirmed by MALDI-TOF-MS (m/z = 8918 $[M + Na]^+$) (Figure 2B).

The self-assembling behavior of $dA_{20}$-modified *β*-annulus peptide in 10 mM phosphate buffer (pH 7.1) was examined by transmission electron microscopy (TEM) observations and dynamic light scattering (DLS) measurements. A TEM image of the aqueous solution of **$dA_{20}$-*β*-annulus** stained with phosphotungstic acid showed the formation of spherical assemblies of approximately 60 nm in diameter (Figure 3A). The average hydrodynamic diameter of the assemblies was determined by DLS experiments to be 98 $\pm$ 63 nm (Figure 3B), which represents a larger size and wider distribution than those of unmodified 24-mer *β*-annulus peptides (INHVGGTGGAIMAPVAVTRQLVGS, 47 $\pm$ 7 nm) [20] and unmodified *β*-annulus Cys peptide (53 ± 13 nm, Figure S1). We have demonstrated that DNA was encapsulated into cationic interior of artificial viral capsid self-assembled from unmodified *β*-annulus peptides [21]. Since there is possibility that some DNAs may interact with cationic N-terminus of *β*-annulus peptides, it seems that **$dA_{20}$-*β*-annulus** assemblies showed broad size distribution. The increase in diameter and distribution is probably due to the modification of $dA_{20}$ on the surface of the artificial viral capsids. To construct complementary artificial viral capsids, we synthesized a $dT_{20}$-modified *β*-annulus peptide conjugate (**$dT_{20}$-*β*-annulus**), according to the method described above; this was purified by reversed-phase HPLC and confirmed by MALDI-TOF-MS (m/z = 8718 $[M]^+$). The TEM image showed that **$dT_{20}$-*β*-annulus** also formed spherical assemblies of approximately 60 nm in diameter (Figure 3C). The DLS of an aqueous solution of **$dT_{20}$-*β*-annulus** also showed an average hydrodynamic diameter of 65 ± 20 nm (Figure 3D), which is comparable to the assembly of **$dA_{20}$-*β*-annulus**. The *ζ*-potential of unmodified *β*-annulus Cys peptide was almost neutral (–2 ± 5 mV) at pH 7.1 (Figure 3E), which is consistent with the surface *ζ*-potentials of the *β*-annulus peptide

at pH 7.0 [21]. In contrast, the $\zeta$-potential of **$dA_{20}$-$\beta$-annulus** was –40 ± 9 mV at pH 7.1 (Figure 3E). These results indicate that the exterior surface of the artificial viral capsid self-assembled from **$dA_{20}$-$\beta$-annulus** was coated with negatively charged $dA_{20}$. Figure 4 shows the concentration dependence of **$dA_{20}$-$\beta$-annulus** on the diameter of the assembly obtained from DLS measurements. At a concentration of 0.15–25 μM, **$dA_{20}$-$\beta$-annulus** formed assemblies with sizes of 18–190 nm, whereas at 50–100 μM, it formed aggregates with sizes of more than 200 nm. Since the critical aggregation concentration of unmodified $\beta$-annulus peptide was 25 μM [20], it is interesting to note that the **$dA_{20}$-$\beta$-annulus** can self-assemble at lower concentrations in spite of the negative charges of DNA. Although mechanism of the stabilization of capsid structures by modification of DNA is still unclear, it is probable that like-charge attractions [25, 26] or hydration forces [27] among DNA chains on the artificial viral capsids contribute to the stability.

Next, the secondary structure of DNA on the artificial viral capsid was analyzed by circular dichroism (CD) spectroscopy. Figure 5A shows the CD spectra of $dA_{20}$, $\beta$-annulus peptide, **$dA_{20}$-$\beta$-annulus**, and the difference spectrum obtained by subtracting $\beta$-annulus peptide from **$dA_{20}$-$\beta$-annulus**. The CD spectrum of $\beta$-annulus peptide (blue) shows weak intensity at 220-300 nm, and the CD spectrum of $dA_{20}$ (green) and difference spectrum (red) are almost overlapped at 220-300 nm. This indicate that the CD intensity of negative peak at 248 nm of $dA_{20}$ was minimally affected by conjugating with $\beta$-annulus peptide. Figure 5B shows the CD spectra of **$dA_{20}$-$\beta$-annulus** in the presence of polydT in equimolar concentrations of nucleobase. Addition of the complementary PolydT to **$dA_{20}$-$\beta$-annulus** in equimolar concentrations of nucleobase (Figure 5B, red) showed a larger negative peak at 248 nm than **$dA_{20}$-$\beta$-annulus** alone (Figure 5B, black), indicating the hybridization. This is almost consistent with the CD spectrum of the mixture of $dA_{20}$ and PolydT (Figure 5B, blue), indicating the formation of a C-type DNA duplex, which is usually observed in DNA sequences consisting of only adenine and thymine.

In order to confirm the hybridization ability of the DNA-modified artificial viral capsids, fluorescence spectra of DAPI (4', 6-diamidino-2-phenylidole dihydrochloride), which enhances the fluorescence intensity by binding to the minor groove of the DNA duplex [28], were measured. Although free DAPI has a weak emission maximum at 461 nm, it shifts to a lower wavelength at 456 nm in the presence of PolydA and PolydT [28]. The fluorescence spectrum of DAPI in the presence of a mixture of $dA_{20}$ and PolydT showed a high fluorescence intensity (Figure 6A (d)), indicating full hybridization. In contrast, the fluorescence intensity of DAPI in the presence of **$dA_{20}$-$\beta$-annulus**/polydT (b) or **$dA_{20}$-$\beta$-annulus**/$dT_{20}$ (c) was smaller than that of spectrum (d), indicating that $dT_{20}$ and polydT were partially hybridized with $dA_{20}$ on the capsids. Figure 6B shows that the

fluorescence intensity of the equimolar mixture of **dA$_{20}$-$\beta$-annulus** and **dT$_{20}$-$\beta$-annulus** was increased by 1.4-fold as compared to the sum of each spectrum (e and f), which suggests that dA$_{20}$ and dT$_{20}$ on the capsids were partially hybridized. This might be caused by the steric hindrance between two DNA-modified capsids.

TEM and DLS of the mixture of **dA$_{20}$-$\beta$-annulus** and PolydT showed the formation of an aggregate with a size of about 500 nm (Figure 7A, B), whereas the mixture of **dA$_{20}$-$\beta$-annulus** and PolydA afforded individual artificial capsids and minimally sized aggregates of capsids (Figure 7C, D). TEM and DLS of the equimolar mixture of **dT$_{20}$-$\beta$-annulus** and PolydA showed the formation of spherical structures with a size of 10–30 nm and partial aggregation (Figure 8A, B). In contrast, such aggregation was not observed in the equimolar mixture of **dT$_{20}$-$\beta$-annulus** and PolydT (Figure 8C, D). These results indicate that DNA displayed on the surface of the artificial viral capsid can recognize the complementary DNA, which induces aggregation of the DNA-coated capsids by crosslinking among capsids with polynucleotide chains. The TEM image and DLS of the equimolar mixture of **dA$_{20}$-$\beta$-annulus** and **dT$_{20}$-$\beta$-annulus** showed the co-existence of two individual capsid assemblies with a size of 62 ± 14 nm and aggregates of these capsids with a size of 304 ± 93 nm (Figure 9). These results suggest that the dA$_{20}$-coated artificial viral capsid can partially hybridize with the complementary dT$_{20}$-coated capsid to form an aggregate.

## Conclusion

We demonstrated the syntheses of C-terminal-modified $\beta$-annulus peptides with dA$_{20}$ and dT$_{20}$. The TEM images of the DNA-modified peptides showed that the peptide conjugates self-assembled into nanocapsules of approximately 45–160 nm in size. The $\zeta$-potential and DNA-hybridization behaviors of the capsids indicated that DNAs were displayed on the surface of the artificial viral capsids. DNA displayed on the artificial viral capsid can recognize the complementary DNA. The present strategy will be extended to the fabrication of artificial viral capsids modified with DNA aptamers and DNA vaccine adjuvants.

## Experimental Section

**General.** Reagents were obtained from a commercial source and used without further purification. Ion-exchanged water was used as a solvent for peptides in all experiments. Reversed-phase HPLC was performed at ambient temperature with a Shimadzu LC-6AD liquid chromatograph equipped with a UV/Vis detector (220 nm and 260 nm, Shimadzu

SPD-10AVvp) using Inertsil WP300 C18 (GL Science, 250 × 4.6 mm or 250 × 20 mm) and Inertsil ODS-3 columns (GL Science, 250 × 4.6 mm or 250 × 20 mm). MALDI-TOF mass spectra were obtained on an Autoflex III (Bruker Daltonics) in linear/positive mode with $\alpha$-cyano-4-hydroxycinnamic acid ($\alpha$-CHCA) and 3-hydroxypicolinic acid (3-HPA), with diammonium hydrogen citrate as matrix. UV-vis spectra of DNA-conjugated peptides were measured at 260 nm using a Jasco V-630 with a quartz cell (S10-UV-1, GL Science).

**Synthesis of $\beta$-Annulus Cys Peptide.** Peptide H-Ile-Asn(Trt)-His(Trt)-Val-Gly-Gly-Thr(tBu)-Gly-Gly-Ala-Ile-Met-Ala-Pro-Val-Ala-Val-Thr(tBu)-Arg(Pbf)-Gln(Trt)-Leu-Val-Cys(Trt)-Ser(tBu)-Alko-PEG resin was synthesized on Fmoc-Ser(tBu)-Alko-PEG resin (602 mg, 0.23 mmol/g, Watanabe Chemical Ind. Ltd) using standard Fmoc-based FastMoc coupling chemistry (4 eq. Fmoc-amino acids). A DMF solution of 2-(1*H*-benzotriazole-1-yl)-1, 1, 3, 3-tetramethyluronium hexafluorophosphate (HBTU, 0.5 M) and 1-hydroxybenzotriazole hydrate (HOBt•$H_2O$, 0.5 M) was used as a coupling reagent. Diisopropylamine (2.0 M) in NMP and 20% piperidine in *N*-methylpyrrolidone (NMP) were used for neutralization and for Fmoc deprotection, respectively. The peptidyl resin was washed with NMP and then dried under vacuum. The peptide was deprotected and cleaved from the resin by treatment with a cocktail of trifluoroacetic acid (TFA)/1, 2-ethanedithiol/triisopropylsilane/water = 9.5/0.25/0.1/0.25 (mL) for 3 h at room temperature. The reaction mixture was filtered to remove the resin and the filtrate was concentrated under vacuum. The peptide was precipitated by adding ice-cooled methyl-*tert*-butyl ether (MTBE) to the residue and the supernatant was decanted. After repeating the MTBE washing 3 times, the precipitated peptide was dried under vacuum. The crude product was purified by reversed-phase HPLC (Inertsil WP300 C18), eluting with a linear gradient of $CH_3CN$/water (25/75 to 55/45 over 90 min) containing 0.1% TFA. The elution fraction containing the desired peptide was lyophilized to give a flocculent solid. The isolated yield was 5.1 mg (13%). MALDI-TOF-MS (matrix: $\alpha$-CHCA): m/z = 2351.0 ($[M]^+$).

**Preparation of DNA-$\beta$-annulus Peptide Conjugates.** An aqueous solution of $dA_{20}$-$(CH_2)_6$-$NH_2$ (0.1 mL of 1.0 mM, Gene Design Inc.) was mixed with 9.1 mg of *N*-(4-maleimidobutyryloxy)-sulfosuccinimide sodium salt (Sulfo-GMBS, 2.4 μmol, 240 equiv.) and 0.5 mL of 0.1 M sodium bicarbonate aqueous solution. The mixture was incubated for 2 h at 25ºC, and then dialyzed with a dialysis membrane (Spectra/por7, cutoff Mw 1,000, Spectrum Laboratories, Inc.) for 20 h in water. The mixture was monitored by reversed-phase HPLC (Inertsil ODS-3), eluting with a linear gradient of $CH_3CN$/0.1 M ammonium formate aqueous solution (0/100 to 100/0 over 105 min). In

order to remove ammonium formate and $CH_3CN$, water was added into the elution fraction and then the frozen mixture was concentrated in a centrifugal evaporator. The procedure was repeated 5 times, and then the product was confirmed by MALDI-TOF-MS (matrix: 3-HPA). After dialysis using Spectra/por7, the maleimide-$dA_{20}$ was lyophilized for the next reaction without further purification. The maleimide-$dT_{20}$ was also obtained by a similar method to that described above by using 0.1 mL of 1.0 mM aqueous solution of $dT_{20}$-$(CH_2)_6$-$NH_2$ (Gene Design Inc.).

The $dA_{20}$-maleimide was dissolved in 0.2 mL of 0.1 M phosphate buffer (pH 6.6). *β*-Annulus Cys peptide (1 mg, 0.47 μmol) in water/acetonitrile (2/3, v/v, 1 mL) was added to the solution and incubated for 48 h at 40ºC. The solution was purified by reversed-phase HPLC (Inertsil ODS-3), eluting with a linear gradient of $CH_3CN$/0.1 M ammonium formate aqueous solution (0/100 to 100/0 over 105 min). The elution fraction was collected, the frozen mixture was concentrated in a centrifugal evaporator, and then the mixture was dialyzed using a dialysis membrane (Spectra/por7, cutoff Mw 1,000, Spectrum Laboratories, Inc.) for 20 h with water. The internal solution was lyophilized to give a flocculent solid. After dissolving in water, the concentration of the product was determined from the absorbance at 260 nm. The yield of **$dA_{20}$-*β*-annulus** was 55 nmol (23.6%). MALDI-TOF-MS (matrix: 3-HPA): m/z = 8918 ($[M + Na]^+$). The $dT_{20}$-modified *β*-annulus peptide (**$dT_{20}$-*β*-annulus**) was also prepared according to the method described above. The yield of the product was 21 nmol (22.2%). MALDI-TOF-MS (matrix: 3-HPA): m/z = 8718 ($[M]^+$).

**Dynamic Light Scattering.** Stock solutions (0.1 mM) of DNA-*β*-annulus peptide conjugates (**$dA_{20}$-*β*-annulus** and **$dT_{20}$-*β*-annulus**) in 10 mM phosphate buffer (pH 7.1) were prepared by dissolution in the buffer. Polydeoxyadenylic acid sodium salt (PolydA, Sigma-Aldrich) was dissolved in 10 mM phosphate buffer (pH 7.1) as a stock solution (2.5 mM). The samples were diluted to equimolar amounts of nucleobase in 10 mM phosphate buffer (pH 7.1) and sonicated for 5 min before DLS measurement. DLS was measured with a Zetasizer NanoZS (MALVERN) instrument at 25ºC using an incident He-Ne laser (633 nm). Correlation times of scattered light intensities $G(\tau)$ were measured several times, and the means were calculated and fitted to equation 1, where $B$ is the baseline, $A$ is the amplitude, $q$ is the scattering vector, $\tau$ is the delay time and $D$ is the diffusion coefficient.

$$G(\tau) = B + A \exp(-2q^2 D\tau) \quad (1)$$

The hydrodynamic radii ($R_H$) of the scattering particles were calculated using the Stokes–Einstein equation (eq. 2), where $\eta$ is the solvent viscosity, $k_B$ is Boltzmann's constant, and $T$ denotes the absolute temperature.

$$R_H = k_B T / 6\pi\eta D \quad (2)$$

**Zeta Potential Analysis.** The zeta potential was measured at 25ºC using a Zetasizer Nano ZS (MALVERN) with a DT1061 clear disposable zeta cell. The **dA$_{20}$-*β*-annulus** and *β*-annulus-Cys peptide were diluted to 25 μM with 10 mM phosphate buffer (pH 7.1) before measurement.

**Transmission Electron Microscopy.** Aliquots (5 μL) of DLS samples were applied to hydrophilized carbon-coated Cu-grids (C-SMART Hydrophilic TEM girds, ALLANCE Biosystems) for 60 s and were then removed. Subsequently the TEM grid was instilled in the staining solution (2% phosphotungstic acid ($Na_3$ ($PW_{12}O_{40}$) $(H_2O)_n$) aqueous solution, 5 μL) for 1 min, and then removed. After the sample-loaded carbon-coated grids were dried *in vacuo*, they were observed by TEM (JEOL JEM 1400 Plus), using an accelerating voltage of 80 kV.

**Fluorescence Spectra.** Sample solutions of **dA$_{20}$-*β*-annulus** (25 μM), **dT$_{20}$-*β*-annulus** (25 μM), and their equimolar mixture were prepared by dissolution in 10 mM phosphate buffer (pH 7.1). Equimolar amounts in a nucleobase concentration of oligodeoxyribonucleotides ($dA_{20}$ and $dT_{20}$, Gene Design Inc.), PolydT (Sigma-Aldrich) and PolydA (Sigma-Aldrich) were also added to the sample solutions. Then, an aqueous stock solution of 4',6-diamidino-2-phenylindole (DAPI, DOJINDO) in10 mM phosphate buffer (pH 7.1) was added to the sample solutions (final concentration of DAPI: 10 μM). The fluorescence spectra were measured with a Jasco FP8200 spectrofluorometer at 25ºC using an excitation wavelength of 345 nm.

**Acknowledgment**

This research was partially supported by The Asahi Glass Foundation and a Grant-in-Aid for Scientific Research (B) from the Japan Society for the Promotion of Science (JSPS KAKENHI, No. 15H03838).

**References**

1. Wen AM, Steinmetz NF. Design of virus-based nanomaterials for medicine, biotechnology, and energy. *Chem. Soc. Rev*. 2016; **45**: 4074-4126.
2. Zeltins A. Construction and characterization of virus-like particles: A Review. *Mol Biotechnol*. 2013; **53**: 92-107.
3. Mateu MG. Virus engineering: functionalization and stabilization. *Protein Eng. Des. Sel.* 2011; **24**: 53-63.
4. Lee SY, Lim JS, Harris MT. Synthesis and application of virus-based hybrid nanomaterials. *Biotechnol. Bioeng*. 2012; **109**: 16-30.

5. Patterson DP, Prevelige PE, Douglas T. Nanoreactors by programmed enzyme encapsulation inside the capsid of the bacteriophage P22. *ACS Nano* 2012; **6**: 5000-5009.
6. Li F, Gao D, Zhai X, Chen Y, Fu T, Wu D, Zhang ZP, Zhang XE, Wang Q. Tunable, discrete, three-dimensional hybrid nanoarchitectures. *Angew. Chem. Int. Ed*. 2011; **50**: 4202-4205.
7. Raja KS, Wang Q, Finn MG. Icosahedral virus particles as polyvalent carbohydrate display platforms. *ChemBioChem* 2003; **4**: 1348-1351.
8. Wickham TJ, Segal DM, Roelvink PW, Carrion ME, Lizonova A, Lee GM, Kovesdi I. Targeted Adenovirus Gene Transfer to Endothelial and Smooth Muscle Cells by Using Bispecific Antibodies. *J. Virol.* 1996; **70**: 6831-6838.
9. Pinheiro1 AV, Han D, Shih WM, Yan H. Challenges and opportunities for structural DNA nanotechnology. *Nature Nanotech.* 2011; **6**: 763-772.
10. Aldaye FA, Palmer AL, Sleiman HF. Assembling materials with DNA as the guide. *Science*. 2008; **321**: 1795-1799.
11. Stephanopoulos N, Liu M, Tong GJ, Li Z, Liu Y, Yan H, Francis MB. Immobilization and one-dimensional arrangement of virus capsids with nanoscale precision using DNA origami. *Nano Lett*. 2010; **10**: 2714-2720.
12. Strable E, Johnson JE, Finn MG. Natural nanochemical building blocks: icosahedral virus particles organized by attached oligonucleotides. *Nano Lett.* 2004; **4**: 1385-1389.
13. Tong GJ, Hsiao SC, Carrico ZM, Francis MB. Viral capsid DNA aptamer conjugates as multivalent cell-targeting vehicles. *J. Am. Chem. Soc*. 2009; **131**: 11174-11178.
14. Matsuura K. Rational design of self-assembled proteins and peptides for nano- and micro-sized architectures. *RSC Adv* 2014; **4**: 2942-2953.
15. McManus JJ, Charbonneau P, Zaccarelli E, Asherie N. The physics of protein self-assembly. *Curr Opin Colloid Interface Sci.* 2016; **22**: 73-79.
16. Fletcher JM, Harniman RL, Barnes FRH, Boyle AL, Collins A, Mantell J, Sharp TH, Antognozzi M, Booth PJ, Linden N, Miles MJ, Sessions RB, Verkade P, Woolfson DN. Self-assembling cages from coiled-coil peptide modules. *Science* 2013; **340**: 595-599.
17. Castelletto V, Santis ED, Alkassem H, Lamarre B, Noble JE, Ray S, Bella A, Burns JR, Hoogenboom BW, Ryadnov MG. Structurally plastic peptide capsules for synthetic antimicrobial viruses. *Chem. Sci.* 2016; **7**: 1707-1711.
18. Noble JE, Santis ED, Ravi J, Lamarre B, Castelletto V, Mantell J, Ray S, Ryadnov MG. A de novo virus-like topology for synthetic virions. *J. Am. Chem. Soc*. 2016; **138**: 12202-12210.

19. Murata M, Narahara S, Kawano T, Hamano N, Piao JS, Kang JH, Ohuchida K, Murakami T, Hashizume M. Design and function of engineered protein nanocages as a drug delivery system for targeting pancreatic cancer cell via neuropilin-1. *Mol. Pharm.* 2015; **12**: 1422-1430.
20. Matsuura K, Watanabe K, Matsuzaki T, Sakurai K, Kimizuka N. Self-assembled synthetic viral capsids from a 24-mer viral peptide fragment. *Angew. Chem. Int. Ed.* 2010; **49**: 9662-9665.
21. Matsuura K, Watanabe K, Matsushita Y, Kimizuka N. Guest-binding behavior of peptide nanocapsules self-assembled from viral peptide fragments. *Polym J* 2013; **45**: 529-534.
22. Matsuura K, Nakamura T, Watanabe K, Nogushi T, Minamihata K, Kamiya N, Kimizuka N. Self-assembly of Ni-NTA-modified β-annulus peptides into artificial viral capsids and encapsulation of His-tagged proteins. *Org. Biomol. Chem*. 2016; **14**: 7869-7874.
23. Fujita S, Matsuura K. Encapsulation of CdTe quantum dots into synthetic viral capsids. *Chem. Lett*. 2016; **45**: 922-924.
24. Matsuura K, Ueno G, Fujita S. Self-assembled artificial viral capsid decorated with gold nanoparticles. *Polym J* 2015; **47**: 146-151.
25. Martín-Molina A, Luque-Caballero G, Faraudo J, Quesada-Pérez M, Maldonado-Valderrama J. Adsorption of DNA onto anionic lipid surfaces. *Adv. Colloid Interface Sci.* 2014; **206**: 172-185.
26. Kurona M, Arnold A. Role of geometrical shape in like-charge attraction of DNA. *Eur. Phys. J. E* 2015; **38**: 20.
27. Reddy MR, Berkowitz M. Hydration forces between parallel DNA double helices: Computer simulations. *Proc. Nati. Acad. Sci. USA* 1989; **86**: 3165-3168.
28. Tanious FA, Veal JM, Buczak H, Ratmeyer LS, Wilson WD. DAPI (4',6-Diamidino-2-phenylindole) Binds Differently to DNA and RNA:Minor-Groove Binding at AT Sites and Intercalation at AU Sites. *Biochemistry* 1992; **31**: 3103-3112.

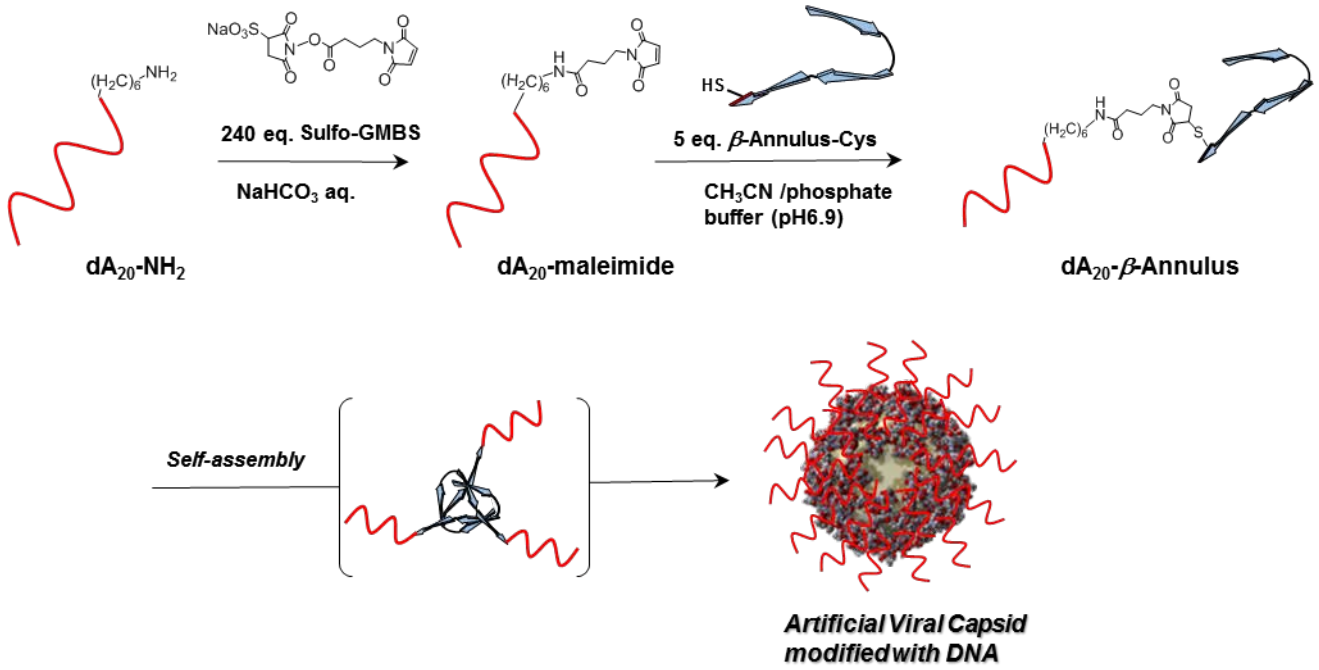


**Figure 1.** Schematic of synthesis of $dA_{20}$-modified $\beta$-annulus peptide (**$dA_{20}$-$\beta$-annulus**) and formation of the $dA_{20}$-modified artificial viral capsid by self-assembly.

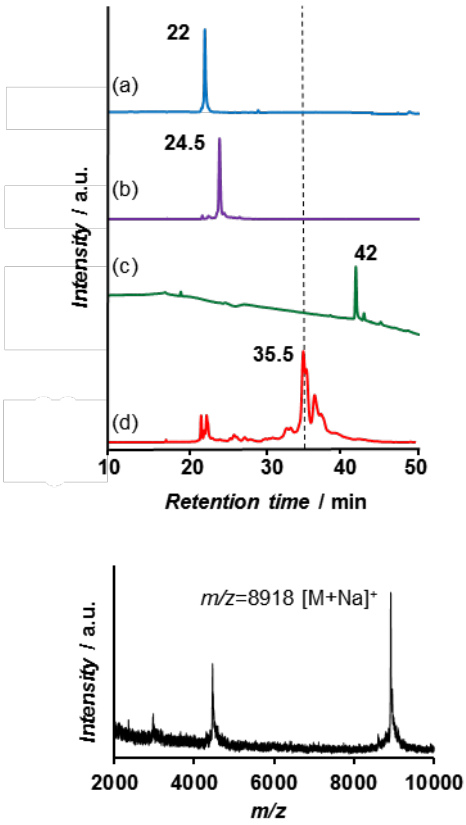


**Figure 2.** (A) Reverse-phase chromatograms of (a) $dA_{20}$-$NH_2$ detected at 260 nm, (b) $dA_{20}$-maleimide detected at 260 nm, (c) *β*-annulus Cys peptide detected at 220 nm, (d) reaction mixture containing **$dA_{20}$-*β*-annulus** detected at 260 nm. (B) MALDI-TOF-MS of the purified **$dA_{20}$-*β*-annulus** (m/z = 8918$[M + Na]^+$).

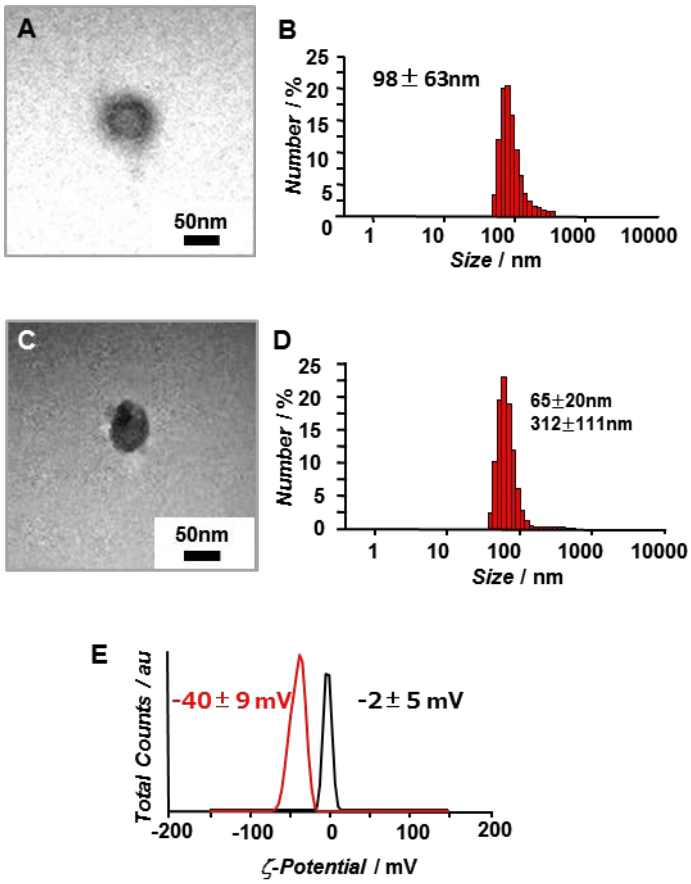


**Figure 3.** TEM images and size distributions obtained from DLS for aqueous solutions of 25μM **$dA_{20}$-*β*-annulus** (A, B) and 25μM **$dT_{20}$-*β*-annulus** (C, D) in phosphate buffer (pH7.1) at 25ºC. (E) Zeta potential of un-modified *β*-annulus Cys peptide (25μM, black) and **$dA_{20}$-*β*-annulus** (25μM, red) measured in 10mM phosphate buffer (pH7.1) at 25ºC.

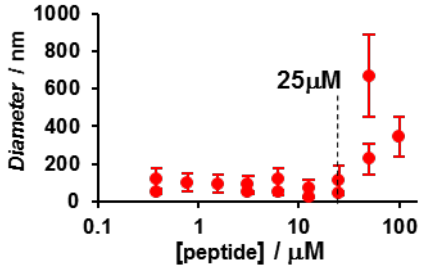


**Figure 4.** Concentration dependence of **dA$_{20}$-*β*-annulus** on the diameter of the assembly obtained from DLS in 10 mM phosphate buffer (pH 7.1) at 25ºC.

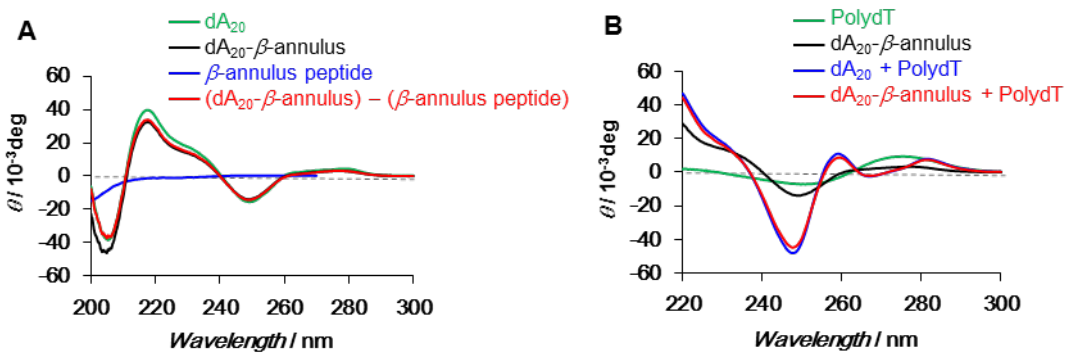


**Figure 5.** CD spectra of (A) $dA_{20}$ (green), **$dA_{20}$-*β*-annulus** (black), *β*-annulus peptide (blue) and the spectrum subtracting *β*-annulus peptide from **$dA_{20}$-*β*-annulus** (red), and (B) **dA20-*β*-annulus** (black), PolydT (green), mixture of $dA_{20}$ and PolydT (blue) and mixture of **$dA_{20}$-*β*-annulus** and PolydT (red) in 10mM phosphate buffer (pH7.1) at 25ºC; [A]=[T]=0.5mM.

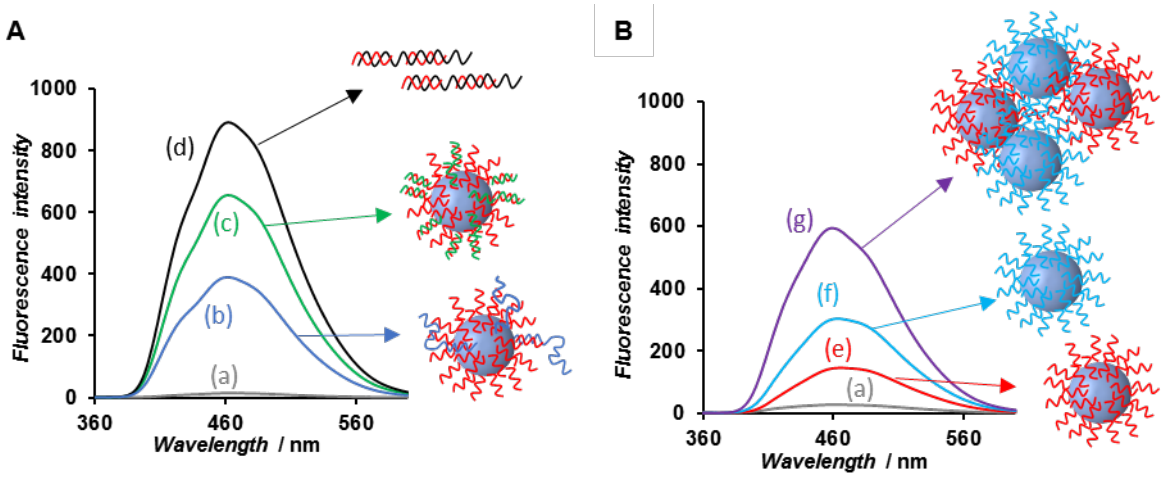


**Figure 6.** Fluorescence spectra of 10 μM DAPI solutions in 10 mM phosphate buffer (pH 7.1, excitation wavelength: 345 nm). (a) DPAI alone, (b) DAPI + 25 μM **$dA_{20}$-*β*-annulus** and PolydT, (c) DAPI + 25 μM **$dA_{20}$-*β*-annulus** and 25 μM $dT_{20}$, (d) DAPI + 25 μM $dA_{20}$ and PolydT, (e) DAPI + 25 μM **$dA_{20}$-*β*-annulus**, (f) DAPI + 25 μM **$dT_{20}$-*β*-annulus**, (g) DAPI + 25 μM **$dA_{20}$-*β*-annulus** and 25 μM **$dT_{20}$-*β*-annulus**. All the nucleobase concentrations are the same: [A] = [T] = 0.5 mM.

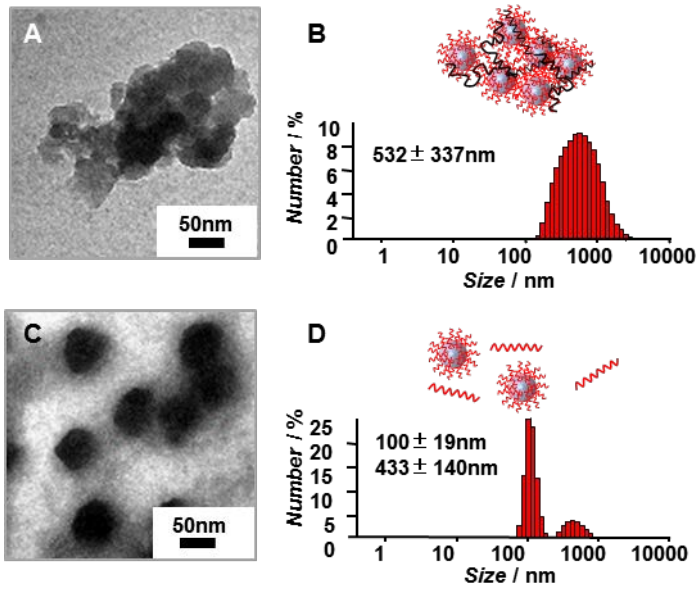


**Figure 7.** TEM images and size distributions obtained from DLS for an aqueous solution of **dA$_{20}$-*β*-annulus** (25 μM) in 10 mM phosphate buffer (pH 7.1) at 25°C. (A, B) in the presence of PolydT ([nucleobase] = 0.5 mM), (C, D) in the presence of PolydA ([nucleobase] = 0.5 mM). TEM images stained with sodium phosphotungstate.

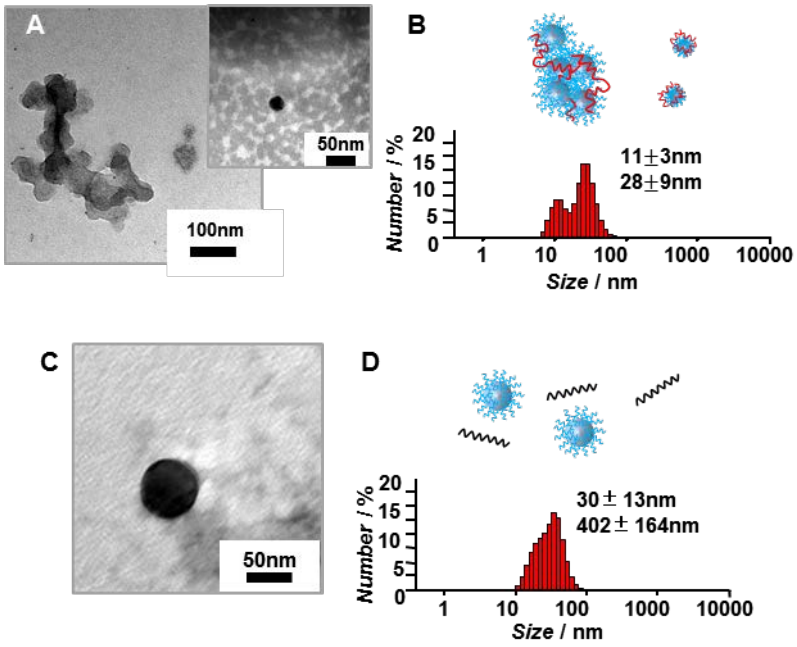


**Figure 8.** TEM images and size distributions obtained from DLS for an aqueous solution of **$dT_{20}$-$\beta$-annulus** (25 μM) in phosphate buffer (pH 7.1) at 25ºC. (A, B) in the presence of PolydA ([nucleobase] = 0.5 mM), (C, D) in the presence of PolydT ([nucleobase] = 0.5 mM). TEM images stained with sodium phosphotungstate.

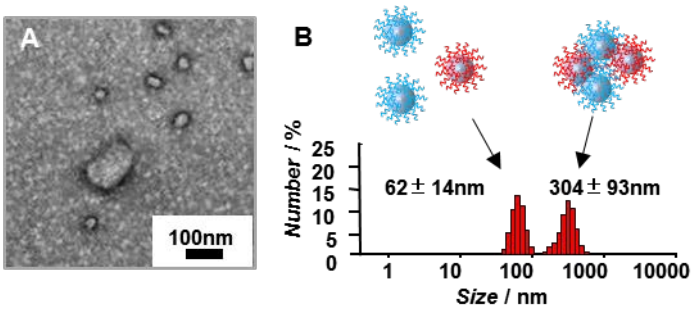


**Figure 9.** TEM image (A) and size distributions obtained from DLS (B) for an aqueous solution of **dA$_{20}$-*β*-annulus** (25 μM) mixed with **dT$_{20}$-*β*-annulus** (25 μM) in 10 mM phosphate buffer (pH 7.1) at 25ºC. TEM images stained with sodium phosphotungstate.